IEEE Access
Multidisciplinary ⋮ Rapid Review ⋮ Open Access Journal

Received 20 November 2023, accepted 8 December 2023, date of publication 2 January 2024,
date of current version 11 January 2024.

Digital Object Identifier 10.1109/ACCESS.2023.3349351

RESEARCH ARTICLE

The Research on Fault Identification of Spatiotemporal Location With Compressed Grid Data Using the Stochastic Sliding Blocks

TAO LIU[1], JIAQING MA[1], CHANGSHENG CHEN[1], TAO QIN[1], ZHIQIN HE[1], QINMU WU[1], AND HUI LONG[2]
[1]College of Electrical Engineering, Guizhou University, Guiyang 550025, China
[2]China Unicom Anshun Branch Office, Anshun 561000, China

Corresponding author: Jiaqing Ma (357287962@qq.com)

This work was supported in part by the National Natural Science Foundation of China under Grant 62163006; and in part by the Guizhou Provincial Science and Technology Department under Grant PGTS[2021]G442, Grant [2022]G244, Grant [2023]G096, and Grant [2023]G179.

ABSTRACT To identify the compressed power grid fault data quickly and effectively, this paper presents a spatiotemporal location fault diagnosis method for the data compressed with set partitioning in hierarchical trees (SPIHT) algorithm. Firstly, the data from the multi-channel collector is constructed into a two-dimensional grey-scale digital image and compressed with the improved SPIHT algorithm. Then, the peak signal-to-noise ratio (PSNR) parameter of the compressed data is considered to identify the abnormal data. Finally, a random sliding block is used to scan and process each block of power grid data during the abnormal time range. The abnormal data block of power grid data is identified by analyzing the compression parameters of power grid data processed by each block. The node corresponding to the abnormal data block is found, and the power grid fault data is in space. Simulation and experimental results verify the correctness and effectiveness of the proposed method.

INDEX TERMS Power grid data, spatiotemporal, PSNR, fault time location, fault space location.

I. INTRODUCTION

With the development of the energy Internet, the scale of the system is becoming larger and larger. Massive data information is generated due to the stable and efficient operation of the power grid system [1], [2], [3]. In order to reduce the data information storage and reduce the cost, it is necessary to compress the power grid data, which is conducive to storage and transmission. Effective data compression methods are considered to compress power data for reducing or solving the above problems [4], [5], [6]. The goal of the compression method is to reduce the size of the data, and the compressed data contains the main features of the original information. Data compression can be divided into lossless and lossy compression, and researchers are actively proposing effective data compression methods [7], [8], [9].

Many different lossy compression methods have been applied to smart grids. In the smart grid, the multi-resolution characteristics of wavelets are used to solve the data storage problem effectively [10]. Ning et al. [11] proposed a wavelet-based data compression method for an intelligent grid. The data compression and denoising ability of power system signal by multi-resolution analysis based on wavelet transform is studied. According to the maximum wave energy criterion of the wavelet coefficient, the second-order multi-wave and fifth-order multi-wave are selected as the best wavelet function and the best decomposition scale of the disturbed signal. Jose and Morsi [12] used wavelet

The associate editor coordinating the review of this manuscript and approving it for publication was Wencong Su.

multi-resolution signal decomposition into different decomposition levels for data compression under the condition that the transmission capacity of the communication network was met and then applied threshold values at each wavelet decomposition level to capture the features required for signal reconstruction. Liu et al. [13] used the signal's sparsity to linearly project the transformation coefficient into the low-dimensional observation vector and accurately reconstruct the original signal with high probability by further solving the sparse optimization. Based on KSVD, a sparse matrix training algorithm based on block power data is designed.

In addition, lossless compression methods for data compression applications have also emerged, primarily to delete redundant data [14], reduce memory space, improve transmission speed, and improve bandwidth utilization. Embedded Zero tree Wavelet (EZWT) is a simple and effective data compression algorithm that does not need training, pre-storage, or prior knowledge of the data source. Khan et al. [15] proposed an intelligent grid data denoising and compression technology based on the EZWT transform to analyze power system signals and study the performance of compression and noise reduction. Xin et al. [16] proposed a power data imaging and power data image compression and reconstruction method based on EZWT image coding. EZWT coding was adopted to combine zero-tree structure with SAQ to compress and decompress power data images in the image compression and reconstruction mechanism. The compression of power grid data is mainly studied and experimented with a two-dimensional image compression method, SPIHT algorithm [17]. SPIHT is an improved scheme of EZW, and its effect is better than the EZW algorithm [18]. It adopts the structure of a spatial direction tree to transmit important nodes first [19]. Make full use of the characteristics of wavelet coefficients in different frequency bands and carry out sequential quantization encoding of wavelet coefficients [20]. A block-based parallel SPIHT algorithm improves the algorithm's speed while reducing the image compression effect, which reduces PSNR [21]. The image compression algorithm based on the improved image block classification algorithm can preserve the detailed information more effectively after image compression. This algorithm can reduce engineering applications' transmission bandwidth and storage space [22]. In the paper, the improved compression algorithm of SPIHT is used to compress the power grid data efficiently. The algorithm saves storage space by improving its PSNR. So, the fault points of abnormal data are judged, and the method's feasibility is verified by experiment and simulation.

The main contribution of this work is to propose an improved SPIHT compression algorithm using the stochastic sliding block based on the characteristics of power grid data compression introduced fault power grid data spatiotemporal location method. The paper is organized as follows: firstly, the improved SPIHT algorithm is presented; then, the architecture of the power grid data model is introduced. Finally, the simulation experiment and result analysis of fault diagnosis concludes the paper with a discussion of possible directions to improve the proposed approach.

II. ASPIHT METHOD

SPIHT is an embedded image compression coding based on the wavelet coefficients processed after wavelet transform. It uses the spatial direction tree to describe the relationship between each sub-band [23]. In the SPIHT algorithm, each coefficient corresponds to the spatial tree node; coordinates (r, c) are used to identify the node, and $c_{r,c}$ represents the wavelet coefficient. In the spatial orientation tree, for the image after the n-level wavelet transform, where the horizontal direction $HL_1, HL_2, \cdots, HL_N$ subbands are divided into a set, the vertical direction $LH_1, LH_2, \cdots, LH_N$ subbands are divided into a set, the diagonal direction $HH_1, HH_2, \cdots, HH_N$ subbands are divided into a set, and the lowest frequency subband LL_N is divided into a set separately. The spatial direction tree structure of the SPIHT algorithm is shown in Fig. 1.

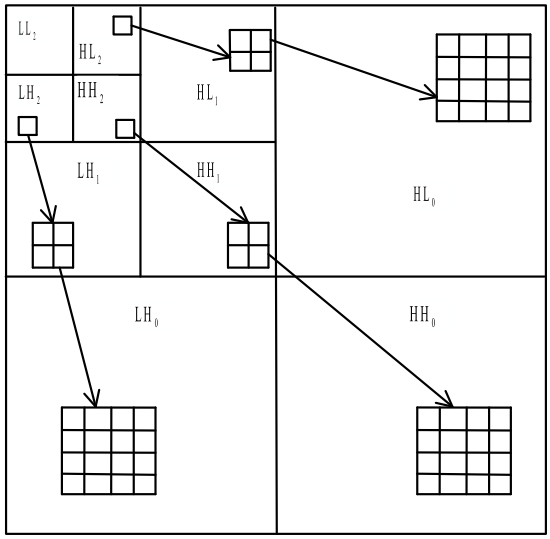

FIGURE 1. Spatial direction tree structure.

In multi-resolution space [24], it is to divide the frequency space of the sampled signal. The original signal is divided into low-frequency and high-frequency by low-pass and high-pass filters. Low frequency reflects the general picture, and high frequency represents the details of the original signal. SPIHT algorithm introduces LIP, LSP, and LIS lists as encoding and decoding control, representing non-important pixel lists, essential coefficient lists, and non-important set lists, respectively. The coding process of the SPIHT algorithm includes five key steps: initialization, scan sorting, element checking, fine scanning, and updating threshold [19], [25], [26], [27], [28].

Step 1: Initialize LSP, LIP, and LIS and set the threshold to T0.

Step 2: By scanning the LIP list coefficients, the wavelet coefficients in this coordinate system are divided into

unimportant and essential coefficients. If the coefficient is unimportant, output '0' directly to the sort stream and remain in the LIP table. Suppose it is a crucial coefficient, then output '1' to the sort stream. In the critical coefficient, if it is a positive significant coefficient, it is represented by '1'; if it is a negative significant coefficient, it is represented by '0'. The significant coefficients are removed from the LIP table and added to the tail of the LSP.

Step 3: The collection elements in the LIS list are scanned by classification. LIS table contains $D(r, c)$ and $L(r, c)$ sets. Importance judgment and scanning are carried out for the two sets.

Step 4: Fine scanning;

Step 5: Update the threshold. Halve the threshold for the following scan.

The research and analysis of the SPIHT algorithm show that it still has some defects. This paper mainly improves the algorithm from the following aspects:

(1) A specific correlation exists between adjacent elements in the same subband. SPIHT algorithm uses the threshold method to encode the coefficients progressively. It divides the threshold by two each time to get a new threshold for re-coding and sorting so that whether the coefficients fluctuating near the threshold can be encoded affects the quality of the current decoded image. At a low bit rate, the reconstructed image has more distortion and poor visual effects.

(2) The same coding method is used for different frequency domains so that the high-low band system obtained by wavelet transform (low-frequency subband represents the approximate part of the image, and the coefficient is generally significant; The high-frequency subband represents the detailed part of the image, and the coefficient is generally tiny).

(3) There is still some data redundancy in the SPIHT algorithm. When too many unimportant coefficients exist, coding time increases and coding speed is reduced.

Based on the above mentioned, a predictive coding algorithm is used to improve the SPIHT algorithm by using element correlation, and different coding methods are used in different frequency domains so that it can better reconstruct images and enhance visual effects. The primary step of prediction coding is first to construct the prediction formula, then calculate the error of the predicted value, and then encode its error. Differential pulse code modulation (DPCM) is one of the most commonly used linear predictive coding algorithms in practical applications, and its coding process is shown in Fig. 2.

DPCM linear prediction is mainly based on Markov's prototype, which uses the high correlation between adjacent pixels in the original signal data and uses one pixel scanned by the Markov model to predict the value of another pixel [29], [30], [31], [32]. The key idea of DPCM prediction is to predict each pixel value of the original signal data so that the entropy of the original signal after a series of predictions is less than the original entropy. For DPCM prediction coding of images, the prediction model is designed according to the correlation

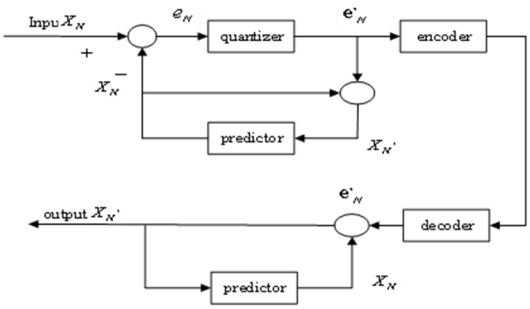

FIGURE 2. DPCM principle.

between adjacent pixels, expressed by the following formula:

$$X_k = \sum_{i=1}^{N} c_i X_{(k-i)} \tag{1}$$

For the target sample points to be predicted, we can select the 12 adjacent values of the scan row and column that are closest to the target sample and have the highest correlation with the target sample to predict the target sample points and then design the prediction parameters before the adjacent pixel values of the DPCM prediction model according to the correlation between the target sample points and these 12 adjacent pixels. In order to simplify the complexity of the algorithm and predict more appropriate predicted values, this paper selects four adjacent pixel values for prediction, and the DPCM prediction model designed in this paper is shown as follows:

$$\begin{aligned} X(k+1, l+1) = X(k+1, l+1) \\ - [\frac{1}{2} \times X(k+1, l) + \frac{1}{4} \times X(k, l+1) \\ + \frac{1}{8} \times X(k, l) + \frac{1}{8} \times X(k, l+2)] \end{aligned} \tag{2}$$

The relationship between pixel values is shown in Fig. 3.

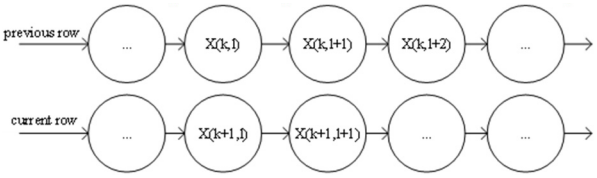

FIGURE 3. Relationship between pixel.

The specific steps are as follows:

(1) Firstly, the input graphics are respectively transformed by wavelet. The selected wavelet function here is the 9/7 wavelet filter function, and the decomposition series of wavelet transform is selected as three levels. The original input image is decomposed into high and low-frequency subbands by wavelet decomposition: LL_3, HL_3, LH_3, HH_3, HL_2, LH_2, HH_2, HL_1, LH_1, and HH_1.

(2) An upward rounding calculation of the high and low-frequency wavelet coefficients after wavelet transformation is made so that some coefficients slightly smaller than

the threshold of the wavelet coefficients under the current threshold can be encoded so that the image can be compressed and the reconstruction effect of the image at different bit rates can be improved.

(3) Since the coefficients of the low-frequency part represent most of the information of the image, while the original SPIHT algorithm adopts the encoding method of equally important information for both high and low-frequency subband coefficients, it is considered to carry out lossless compression coding algorithm DPCM predictive coding for LL_3 (low-frequency subband), so that most of the information of the image can be preserved without loss. Thus, the quality of image reconstruction can be improved.

(4) It can be seen from the original SPIHT coding process that the coefficients of the sub-high frequency subband are scanned and coded one by one. Therefore, when there are too many unimportant coefficients, there will be unnecessary output bits, so a simple binary tree coding is used here to reduce coding redundancy.

III. CONSTRUCTION OF GRID DATE MODEL

In the power systems research, the power grid simulation model is built by software. We chose the Simulink system based on MATLAB to build a simulation model of the power grid in the paper. The power grid data is obtained by simulation. The compression and application of power grid data are explored based on the SPIHT compression algorithm. The nodes diagram of the grid model is designed and built in this paper. As shown in Fig. 4. There are eight nodes in the figure. The simulated power grid data are obtained by monitoring its nodes.

As shown in Fig. 4, the power grid model mainly includes a generator, transformer, LC filter, load and transmission line. The current, voltage, active power, reactive power, frequency and phase angle values of the six nodes 1,2,3,4,6,8 are monitored and outputted as power grid system data for the SPIHT data compression method. And then, the measurement data from oscilloscopes are formed into a two-dimensional data graph.

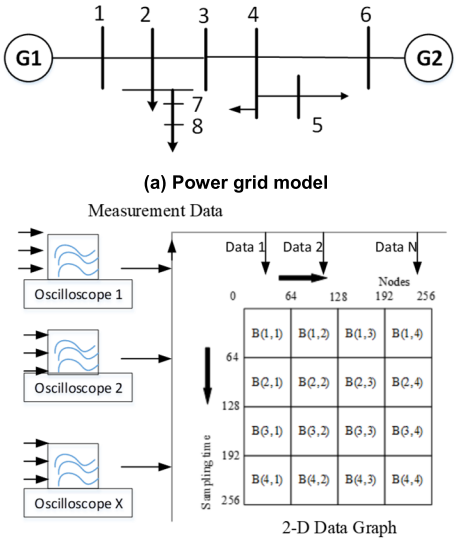

(a) Power grid model

(b) The formation of the grid 2-D data graph data

FIGURE 4. Power grid model and the formation of the data.

IV. RESULT ANALYSIS OF FAULT IDENTIFICATION

This paper simulated the abnormal data of multiple nodes, including the abnormal conditions of slight increase, significant increase and sudden zero change. Two-dimensional normal and abnormal power grid data images generated by model simulation are shown in Fig. 5. Each graph corresponds to the 2-D Data Graph in Fig. 4 (b), where the sampling time is represented vertically from top to bottom, and the node data is represented horizontally from left to right.

It can be seen that the abnormal power grid data image obtained by the simulation is less smooth than the original typical power grid data image. The result parameters of image compression and reconstruction can be used to judge whether the data is abnormal. In image compression, the peak signal-to-noise ratio between the original image and the reconstructed image is often used as an objective evaluation index to evaluate the quality of the compressed image [33], [34].

Assume that $f(x, y)$ is the input image,$x = 0, 1, \cdots, M-1, y = 0, 1, \cdots, N-1$, and $h(x, y)$ represents the decoded image obtained after the input image $f(x, y)$ is compressed and reconstructed. The error of any pixel point between the original image and the compressed reconstructed image is defined as:

$$e(x, y) = h(x, y) - f(x, y) \tag{3}$$

The root mean square error between the original image and the compressed reconstructed image is defined as:

$$MSE = \frac{1}{MN} \sum_{x=0}^{M-1} \sum_{y=0}^{N-1} \left[\hat{f}(x, y) - f\ (x, y) \right]^2 \tag{4}$$

If $f_{max} = \max [f\ (x, y)], x = 0, 1, \ldots, M-1; y = 0, 1, \ldots, N-1$, the peak signal-to-noise ratio is defined as: $PSNR = 10lg \left\{ \frac{f_{max}^2}{MSE} \right\}$.

For 8-bit continuous grayscale images,$f_{\max} = 255$, then $PSNR = 10lg \left\{ \frac{255^2}{MSE} \right\}$

A. FAULT TIME IDENTIFICATION

In the paper, the improved SPIHT method is used to process the original and abnormal power grid data obtained by simulation, respectively. In the experimental simulation, the disturbance is added within 0.03∼0.04s. The simulation results show that after using the SPIHT method to compress and restore, the image quality of the average power grid data is higher, and the distortion rate is lower than that of the abnormal power grid data, which is the purpose of compression and restoration. The characteristic compares the

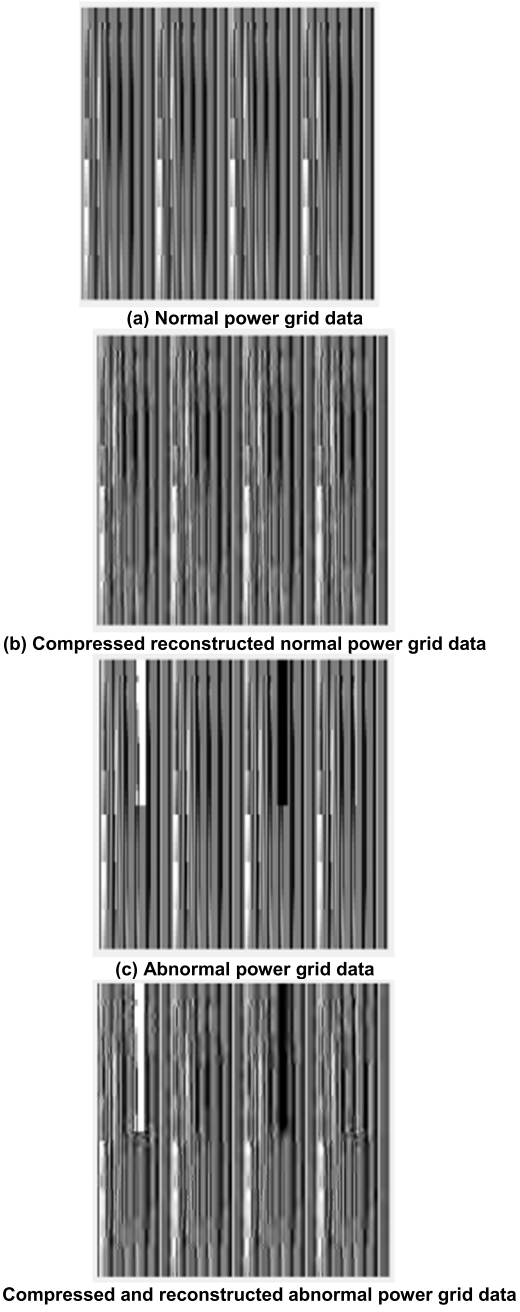

FIGURE 5. Normal and abnormal power grid data images.

PSNR of normal and abnormal power grid data obtained at different bit rates (BR) of power grid data images in different time periods. Here, only power grid data of three power frequency cycles in the first 0.06s is analyzed and displayed. The experimental results are shown in Table 1.

As shown in Table 1, after the power grid data, images in the time interval of 0.02s, 0.04s and 0.06s are compressed by the SPIHT method. The PSNR of the original power grid data and the fault power grid data at different bit rates are significantly different. For example, PSNR are 12.0858, 13.9075, 18.4163, and 19.8959 at the bit rates of 0.25, 0.5, 0.75, and 1,

TABLE 1. PSNR of normal power grid data and abnormal power grid data within 0 to 0.06s.

Bit rate /bps	Normal data	0~0.02s	0.02~0.04s	0.04~0.06s
0.25	12.0858	12.0858	5.4115	12.1929
0.5	13.9075	13.9075	11.8288	14.0042
0.75	18.4163	18.4163	13.6862	18.3407
1	19.8959	19.8959	17.1677	19.9454

respectively, PSNR at the bit rates of 0.25, 0.5, 0.75 and 1 in the interval of 0.02-0.04s are 5.4115, 11.8288, 13.6862 and 17.1677 respectively. It can be seen from Fig. 6 that the PSNR of power grid data compressed and reconstructed at the time interval of 0.03-0.04s are significantly different from that of standard power grid data. Therefore, according to the characteristic, it can be judged that the power grid data at the time interval of 0.02-0.04s are abnormal. According to the method, the effect of faulty time interval location can be achieved.

B. FAULT SPACE IDENTIFICATION

For the faulty space identification method, the judgment method of the time node is used to find the time period of the fault power grid data. During the faulty time interval, continue to judge the fault data occurred in which spatial nodes among the data collected.

In order to find the spatial fault nodes, the method compresses and reconstructs power grid data blocks, which are obtained from the original power grid data and in the faulty time interval. Each data block's compression and reconstruction effects are analyzed and compared, respectively. In order to find faulty space nodes quickly, the partitioned matrix is labelled according to coordinates. The specific dividing blocks method and dividing symbol are shown in Fig. 7.

The 256 $\times$ 256 images represent the power grid data acquired in each power frequency cycle (data collected per 0.02s). In the Fig. 7, the B(1,1) represents the block with coordinates (1,1). The method of dividing blocks divides it into 16 64 $\times$ 64 blocks. The 256 $\times$ 256 power grid data image is divided into 16 data blocks. Each block is marked with a separate coordinate so that it can locate the abnormal data block quickly. They set the stochastic sliding block to scan by taking coordinate blocks from left to right and top to bottom. Each block is analyzed separately to determine whether there are abnormalities to narrow the space of fault location judgment.

As shown in Fig. 8, the coordinates (i,j), (i,j-1), (i-1,j), (i,j+1) and (i+1,j) of data blocks are represented as 1,2,3,4 and 5. In the power grid model, the horizontal coordinate of the corresponding matrix represents the data collected by the oscilloscope of the corresponding node. Moreover, the vertical coordinate represents the corresponding sampling time in the two-dimensional power grid data. In order to find spatial nodes quickly, we mark each oscilloscope corresponding to

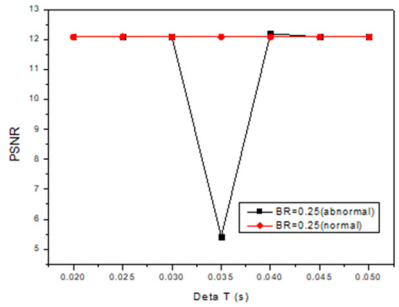

(a) BR=0.25bps

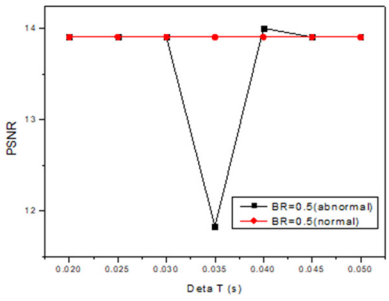

(b) BR=0.5bps

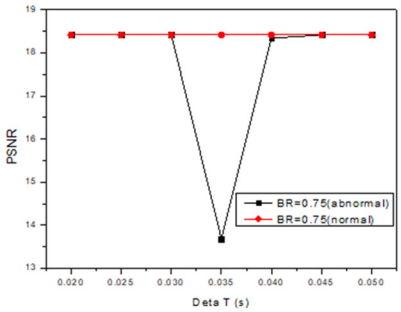

(c) BR=0.75bps

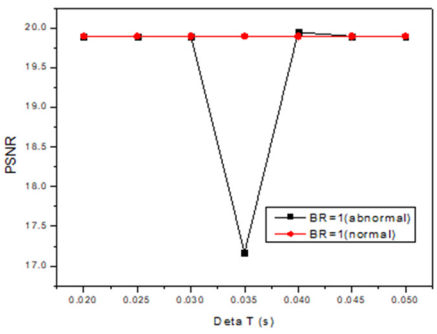

(d) BR=1bps

FIGURE 6. PSNR trend of power grid data image and normal power grid image compression and reconstruction.

power grid data with corresponding numbers. When we judge that the block marked only by the (i, j) coordinate is a fault data block, we can judge that the fault data only appears in the oscilloscope marked by the ordinate corresponding to the faulty block. If continuous data blocks occur, such as (i-1, j),

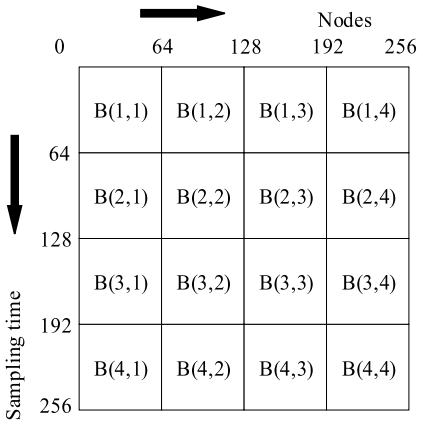

FIGURE 7. Power grid data block marking diagram.

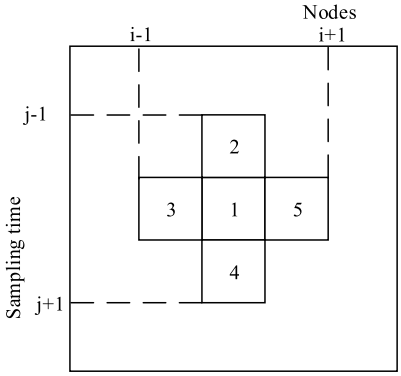

FIGURE 8. Example of fault location in space.

(i, j) and (i+1, j) respectively marked with coordinates are faulty data blocks. Then, the oscilloscope marked with fault data in the range of (i-1) ∼ (i+1) can be identified. To quickly find faulty oscilloscope space nodes and scope. We need an in-depth analysis of the corresponding oscilloscope nodes' fault power grid data and diagnostic failure reason. Then, the equipment can quickly be restored to customary conditions to reduce the loss caused by abnormal power. According to the corresponding faulty diagnosis results, the corresponding technology is used to reduce the occurrences of abnormal times. The method can also unceasingly reduce the time range of the fault data based on fault time judgment.

The above method is used to analyze the experimental data. The peak signal-to-noise ratio was compared at different bit rates under different marker blocks. The simulation experimental data are shown in Table 2. and Table 3.

As shown in Table 2. under different coordinate blocks (CB), the PSNR of the original and fault power grid data at different bit rates are relatively close; there are no apparent differences, while some produce significantly different peak signal-to-noise ratios. According to Fig. 9, it can be seen that blocks marked by coordinates (3,1), (3,4), (4,1) and (4,4) are compressed and reconstructed by the SPIHT method. The PSNR of original and fault power grid data are different at different bit rates. It can be judged that the spatial nodes where

TABLE 2. PSNR of normal power grid data after block marking at different bit rates.

coordinate blocks	Bit rates /bps			
	0.25	0.5	0.75	1
(1, 1)	12.2849	14.5573	17.8826	20.6799
(1, 2)	12.7293	15.0482	17.8226	20.5737
(1, 3)	12.7293	15.0482	17.8226	20.5737
coordinate blocks	Bit rates /bps			
	0.25	0.5	0.75	1
(1, 4)	12.7293	15.0482	17.8226	20.5737
(2, 1)	11.5558	13.4589	18.4503	19.1979
(2, 2)	11.9183	13.822	18.514	19.3211
(2, 3)	11.9183	13.822	18.514	19.3211
(2, 4)	11.9183	13.822	18.514	19.3211
(3, 1)	11.381	12.9181	16.334	18.8544
(3, 2)	11.7593	13.3676	16.4763	18.645
(3, 3)	11.7593	13.3676	16.4763	18.645
(3, 4)	11.7593	13.3676	16.4763	18.645
(4, 1)	11.9532	13.7936	18.3604	19.6754
(4, 2)	12.44	14.0341	17.9008	19.6729
(4, 3)	12.44	14.0341	17.9008	19.6729
(4, 4)	12.44	14.0341	17.9008	19.6729

TABLE 3. PSNR of faulty power grid data after block marking at different bit rates.

coordinate blocks	Bit rates /bps			
	0.25	0.5	0.75	1
(1, 1)	12.2849	14.5573	17.8826	20.6799
(1, 2)	12.7293	15.0482	17.8226	20.5737
(1, 3)	12.7293	15.0482	17.8226	20.5737
(1, 4)	12.7293	15.0482	17.8226	20.5737
(2, 1)	11.5558	13.4589	18.4503	19.1979
(2, 2)	11.9183	13.822	18.514	19.3211
(2, 3)	11.9183	13.822	18.514	19.3211
(2, 4)	11.9183	13.822	18.514	19.3211
(3, 1)	0.23948	5.5318	9.3917	12.268
(3, 2)	11.7453	13.2942	17.5896	18.753
(3, 3)	12.1993	13.6714	17.4972	19.3506
(3, 4)	5.4958	11.4465	13.3173	16.5004
(4, 1)	0.74476	6.2379	10.3701	13.7483
(4, 2)	12.3954	14.0492	17.8596	19.5128
(4, 3)	12.7302	14.4749	17.8112	20.3883
(4, 4)	5.2253	12.5606	13.9894	16.9023

abnormal power grid data occurs are located in the sub-block. If we want to find the specific node, we can continue to use the algorithm to divide the sub-block. According to the same

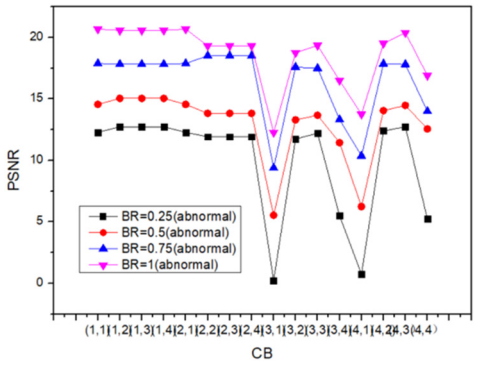

FIGURE 9. PSNR trend of power grid data at different bit rates.

judgment method, we can determine which oscilloscope the abnormal power grid data is obtained from to find the faulty nodes. For example, in the data block marked by coordinate (3,1), PSNR is 11.381, 12.9181, 16.334, 18.8544 when the original power grid data are compressed and reconstructed under 0.25, 0.5, 0.75 and 1-bit rates. However, the PSNR of the fault power grid data are 0.23948, 5.5318, 9.3917 and 12.268. There is an apparent difference between the PSNR of the original and the abnormal power grid data. It can be concluded that a fault occurs in the data block marked by the coordinate (3,1), so the abnormal block is saved for the convenience of analyzing the cause of the fault. Under the data block marked at coordinate (3,2), the PSNR of the original power grid data is 11.7593, 13.3676, 16.4763, 18.645 when the original power grid data are compressed and reconstructed under 0.25, 0.5, 0.75 and 1-bit rates. However, the PSNR of abnormal power grid data are 11.7453, 13.2942, 17.5896 and 18.753. It can be seen that there is no noticeable change in PSNR between the original and abnormal power grid data. Therefore, it can be concluded that there is no abnormal occurrence in the data block marked by the coordinate (3,2), and it is average power grid data. The following blocks should be continued to be judged without saving the data to save memory.

V. CONCLUSION AND DISCUSSION

In the paper, applying the SPIHT compression algorithm to power grid data is an effective method. The SPIHT algorithm and improved SPIHT with stochastic sliding blocks compress the two-dimensional power grid data images. Then, the compression effects of the two algorithms on power grid data images are compared. The experimental results show that both methods have a particular compression effect on power grid data, but the improved SPIHT algorithm can perform better after compression and restoration. They are finally, based on the improved SPIHT algorithm, the characteristics of normal and abnormal power grid data after compression and restoration are analyzed. According to the characteristics, abnormal power grid data quality differs from average power network data after compression and restoration by the SPIHT algorithm. Then, the time period and spatial nodes

of fault power grid data can be located. The experimental results verify the correctness and feasibility of the proposed method.

REFERENCES

[1] Y. Chen, J.-F. Martínez-Ortega, L. López, H. Yu, and Z. Yang, "A dynamic membership group-based multiple-data aggregation scheme for smart grid," *IEEE Internet Things J.*, vol. 8, no. 15, pp. 12360–12374, Aug. 2021.
[2] X. Zhang, C. Huang, Y. Zhang, and S. Cao, "Enabling verifiable privacy-preserving multi-type data aggregation in smart grids," *IEEE Trans. Dependable Secure Comput.*, vol. 19, no. 6, pp. 4225–4239, Nov. 2022.
[3] X. Zhang, C. Huang, C. Xu, Y. Zhang, J. Zhang, and H. Wang, "Key-leakage resilient encrypted data aggregation with lightweight verification in fog-assisted smart grids," *IEEE Internet Things J.*, vol. 8, no. 10, pp. 8234–8245, May 2021.
[4] L. Yan, J. Han, R. Xu, and Z. Li, "Model-free lossless data compression for real-time low-latency transmission in smart grids," *IEEE Trans. Smart Grid*, vol. 12, no. 3, pp. 2601–2610, May 2021.
[5] K. Jia, G. Guo, J. Xiao, H. Zhou, Z. Wang, and G. He, "Data compression approach for the home energy management system," *Appl. Energy*, vol. 247, pp. 643–656, Aug. 2019.
[6] A. Abuadbba, I. Khalil, and X. Yu, "Gaussian approximation-based lossless compression of smart meter readings," *IEEE Trans. Smart Grid*, vol. 9, no. 5, pp. 5047–5056, Sep. 2018.
[7] J. Guo, R. Xie, and G. Jin, "An efficient method for NMR data compression based on fast singular value decomposition," *IEEE Geosci. Remote Sens. Lett.*, vol. 16, no. 2, pp. 301–305, Feb. 2019.
[8] V. Joshi and J. Sheeba Rani, "A simple lossless algorithm for on-board satellite hyperspectral data compression," *IEEE Geosci. Remote Sens. Lett.*, vol. 20, pp. 1–5, 2023.
[9] N. Iqbal, M. Masood, M. Alfarraj, and U. B. Waheed, "Deep seismic CS: A deep learning assisted compressive sensing for seismic data," *IEEE Trans. Geosci. Remote Sens.*, vol. 61, 2023, Art. no. 5913409.
[10] K. H. Talukder and K. Harada, "Multi-threaded concurrent wavelet based image compression and image editing," in *Proc. Int. Conf. Informat., Electron. Vis. (ICIEV)*, May 2012, pp. 822–827.
[11] J. Ning, J. Wang, W. Gao, and C. Liu, "A wavelet-based data compression technique for smart grid," *IEEE Trans. Smart Grid*, vol. 2, no. 1, pp. 212–218, Mar. 2011.
[12] K. M. Jose and W. G. Morsi, "Smart grid data compression of power quality events using wavelet transform," in *Proc. IEEE Can. Conf. Electr. Comput. Eng. (CCECE)*, Halifax, NS, Canada, Sep. 2022, pp. 159–164.
[13] L. Xiaoxiao, T. Jiazheng, and X. Kun, "Low overhead power data acquisition method based on compressed sensing," *Appl. Res. Comput.*, vol. 37, pp. 266–268, Jan. 2019.
[14] G. D. Guglielmo, F. Fahim, C. Herwig, M. B. Valentin, J. Duarte, C. Gingu, P. Harris, J. Hirschauer, M. Kwok, V. Loncar, Y. Luo, L. Miranda, J. Ngadiuba, D. Noonan, S. Ogrenci-Memik, M. Pierini, S. Summers, and N. Tran, "A reconfigurable neural network ASIC for detector front-end data compression at the HL-LHC," *IEEE Trans. Nucl. Sci.*, vol. 68, no. 8, pp. 2179–2186, Aug. 2021.
[15] J. Khan, S. M. A. Bhuiyan, G. Murphy, and M. Arline, "Embedded-zerotree-wavelet-based data denoising and compression for smart grid," *IEEE Trans. Ind. Appl.*, vol. 51, no. 5, pp. 4190–4200, Sep. 2015.
[16] Y. Xin, Q. Xu, Y. Wu, and G. Xue, "Research on power data imaging and compression-reconstruction algorithm," in *Proc. IEEE Sustain. Power Energy Conf. (iSPEC)*, Nanjing, China, Dec. 2021, pp. 2394–2399.
[17] J. Shin and H. Kim, "RL-SPIHT: Reinforcement learning-based adaptive selection of compression ratios for 1-D SPIHT algorithm," *IEEE Access*, vol. 9, pp. 82485–82496, 2021.
[18] Q. Zhang, X. Yuan, and T. Liu, "Blind dual watermarking scheme using Stucki kernel and SPIHT for image self-recovery," *IEEE Access*, vol. 10, pp. 96100–96111, 2022.
[19] E. Christophe, C. Mailhes, and P. Duhamel, "Hyperspectral image compression: Adapting SPIHT and EZW to anisotropic 3-D wavelet coding," *IEEE Trans. Image Process.*, vol. 17, no. 12, pp. 2334–2346, Dec. 2008.
[20] A. L. Souto, V. F. Figueiredo, P. A. Chou, and R. L. de Queiroz, "Set partitioning in hierarchical trees for point cloud attribute compression," *IEEE Signal Process. Lett.*, vol. 28, pp. 1903–1907, 2021.
[21] Y. Jin and H.-J. Lee, "A block-based pass-parallel SPIHT algorithm," *IEEE Trans. Circuits Syst. Video Technol.*, vol. 22, no. 7, pp. 1064–1075, Jul. 2012.
[22] Z. Junxiong and Y. Kai, "Fast Harris corner detection algorithm based on image compression and block," in *Proc. IEEE 10th Int. Conf. Electron. Meas. Instrum.*, vol. 3, Aug. 2011, pp. 143–146.
[23] Y. Yang, M. Cheng, Y. Ding, and W. Zhang, "A visually meaningful image encryption scheme based on lossless compression SPIHT coding," *IEEE Trans. Services Comput.*, vol. 16, no. 4, pp. 2387–2401, Jul. 2023.
[24] F. Palmieri, "A distributed flow correlation attack to anonymizing overlay networks based on wavelet multi-resolution analysis," *IEEE Trans. Dependable Secure Comput.*, vol. 18, no. 5, pp. 2271–2284, Sep. 2021.
[25] C. Li, D. Chen, C. Xie, Y. Gao, and J. Liu, "Research on lossless compression coding algorithm of N-band parametric spectral integer reversible transformation combined with the lifting scheme for hyperspectral images," *IEEE Access*, vol. 10, pp. 88632–88643, 2022.
[26] Z. Fang, N. Xiong, L. T. Yang, X. Sun, and Y. Yang, "Interpolation-based direction-adaptive lifting DWT and modified SPIHT for image compression in multimedia communications," *IEEE Syst. J.*, vol. 5, no. 4, pp. 584–593, Dec. 2011.
[27] S.-C. Tai, C.-C. Sun, and W.-C. Yan, "A 2-D ECG compression method based on wavelet transform and modified SPIHT," *IEEE Trans. Biomed. Eng.*, vol. 52, no. 6, pp. 999–1008, Jun. 2005.
[28] J. Ma, J. Fei, and D. Chen, "Rate-distortion weighted SPIHT algorithm for interferometer data processing," *J. Syst. Eng. Electron.*, vol. 22, no. 4, pp. 547–556, Aug. 2011.
[29] J. Li, J. Wu, and G. Jeon, "GPU acceleration of clustered DPCM for lossless compression of hyperspectral images," *IEEE Trans. Ind. Informat.*, vol. 16, no. 5, pp. 2906–2916, May 2020.
[30] J. Huang and P. P. Mercier, "A 178.9-dB FoM 128-dB SFDR VCO-based AFE for ExG readouts with a calibration-free differential pulse code modulation technique," *IEEE J. Solid-State Circuits*, vol. 56, no. 11, pp. 3236–3246, Nov. 2021.
[31] X. Zhang, R. Min, D. Lyu, D. Zhang, Y. Wang, and Y. Gu, "Current tracking delay effect minimization for digital peak current mode control of DC–DC boost converter," *IEEE Trans. Power Electron.*, vol. 34, no. 12, pp. 12384–12395, Dec. 2019.
[32] O. Ordentlich and U. Erez, "Performance analysis and optimal filter design for sigma-delta modulation via duality with DPCM," *IEEE Trans. Inf. Theory*, vol. 65, no. 2, pp. 1153–1164, Feb. 2019.
[33] C. Zhao, B. Tang, L. Deng, Y. Huang, and Q. Li, "Multilevel adaptive near-lossless compression in edge collaborative wireless sensor networks for mechanical vibration monitoring," *IEEE Trans. Ind. Electron.*, vol. 70, no. 11, pp. 11703–11713, Nov. 2023.
[34] H. Ma, D. Liu, N. Yan, H. Li, and F. Wu, "End-to-end optimized versatile image compression with wavelet-like transform," *IEEE Trans. Pattern Anal. Mach. Intell.*, vol. 44, no. 3, pp. 1247–1263, Mar. 2022.

TAO LIU received the B.S. degree in automation from Guizhou University, where he is currently pursuing the master's degree in control science. His research interests include image processing and fault diagnosis.

JIAQING MA received the B.S. degree from Sichuan Normal University, in 2008, and the Ph.D. degree from Xinan Jiaotong University, in 2014. He is currently an Associate Professor with Guizhou University. His main research interests include the intelligent controller of ac motors and the nonlinear control of power electronics.

CHANGSHENG CHEN received the M.S. degree in engineering from Guizhou University, in 2014. He is currently a Senior Experimentalist with Guizhou University. His main research interests include the industrial robot and embedded systems.

TAO QIN received the M.S. degree from Guizhou University, in 2018. He is currently a Lecturer with Guizhou University. His main research interests include embedded AI computing and smart IoT systems.

ZHIQIN HE received the B.S. degree from Guizhou University, in 2005. She is currently a Professor with Guizhou University. Her main research interests include the intelligent controller of ac motors and the nonlinear control of power electronics.

QINMU WU received the B.S. degree in automation and the M.S. degree in control science and engineering from the Guizhou University of Technology, in 2001, and the Ph.D. degree in control science and engineering from the Huazhong University of Science and Technology, Wuhan, China. He is currently a Professor and a Ph.D. Supervisor with the College of Electrical Engineering, Guizhou University. His current research interests include control theory and applications, networked control, electric vehicle transmission control, and deep learning.

HUI LONG received the B.S. degree from the Qingdao University of Technology, in 2020, and the M.S. degree in engineering from Guizhou University, in 2023. Her research interest includes fault diagnosis.